NASA TECHNICAL MEMORANDUM

NASA TM-73746

NASA TM-73746

INTERIM NOISE CORRELATION FOR SOME OTW CONFIGURATIONS USING EXTERNAL JET-FLOW DEFLECTORS

by U. von Glahn and D. Groesbeck
Lewis Research Center
Cleveland, Ohio 44135

TECHNICAL PAPER to be presented at the
Fourth Aeroacoustics Conference
sponsored by the American Institute of Aeronautics and Astronautics
Atlanta, Georgia, October 3-5, 1977

INTERIM NOISE CORRELATION FOR SOME OTW CONFIGURATIONS USING EXTERNAL JET-FLOW DEFLECTORS

by U. von Glahn and D. Groesbeck

National Aeronautics and Space Administration
Lewis Research Center
Cleveland, Ohio 44135

E-9317

ABSTRACT

Jet/flap interaction acoustic data obtained statically from a model-scale study of STOL-OTW configurations with a conical nozzle mounted above the wing and using various external deflectors to provide jet-flow attachment are correlated. The acoustic data are correlated in terms that consider the jet/flap interaction noise contributions associated primarily with fluctuating lift, trailing edge, and configuration wake noise sources. Variables considered include deflector geometry, flap setting and wing size. Finally, the configuration overall noise levels are related to static lift and thrust measurements in order to provide insight into possible acoustic/aerodynamic performance trade-off benefits.

INTRODUCTION

One method for achieving STOL for aircraft is to mount the engines over the wing and employ external jet-flow deflectors to vector the exhaust flow toward the wing/flap surfaces (fig. 1). Aeroacoustic data obtained at model scale for several such configurations using a conical nozzle are given in reference 1. The variables that were considered in that study included deflector geometry (size and angle setting), flap setting, jet velocity, and wing/flap size.

The present study correlates the jet/flap interaction acoustic results from reference 1. Three jet/flap interaction noise sources are analysed independently in terms of the individual source OASPL and the primary configuration variables. The frequency relationships at which the peak SPL values occur for each noise source are also given. Finally, the overall configuration noise levels are related to the static lift and thrust measurements given in reference 1 in order to guide the assessment of trade-off between acoustic and aerodynamic performance.

The acoustic data were obtained using a conical nozzle with a diameter of 5.2 cm. Flap settings of 20° (takeoff) and 60° (landing) were used with wing chords (flaps retracted) of 33 and 49.5 cm, both

STAR Category 01
AIAA Paper No. 77-1317

having a span of 61 cm (ref. 1). The nozzle was located at 0.1 chord (flaps retracted) downstream of the wing leading edge and 0.1 chord above the wing surface. The wing sizes are referred to herein as baseline (33 cm) and 3/2-baseline (49.5 cm). The acoustic data, including spectral plots, were obtained at far-field radiation angles of 60°, 90°, and 120° measured from the inlet axis. All acoustic data were obtained at nominal cold-flow jet Mach numbers of 0.6 and 0.8. Aerodynamic data obtained included velocity profiles measured at the trailing edge. The lift and thrust force measurements, were presented in reference 1.

APPARATUS AND PROCEDURE

Facilities

Aerodynamic facility. - Thrust and lift forces were obtained at nominal jet exhaust velocities of 200 and 266 m/sec as described and reported in reference 1.

Extensive jet velocity profiles were obtained at the trailing edge of the wing/flap surfaces. Measurements were made with a traversing pitot tube having an entrance cone angle of 60° to help minimize flow angularity effects resulting from the jet flow over the curved surfaces. A vane on the probe was used to set the jet flow angle for each traverse. When the flow angle exceeded the angularity capability of the pitot tube, the tube angle to the local flow was adjusted to provide suitable data. The total pressures measured were plotted directly on an x-y plotter.

Acoustic facility. - The acoustic data were taken at the outdoor facility described in reference 2. In this facility, dry pressurized, ambient temperature air was supplied to the nozzle/wing configurations through a control valve and valve-noise quieting system. This system consisted of a perforated plate, a four-chamber baffled muffler, and approximately 4.6 m of 10.16 cm diameter piping.

Acoustic data were obtained with a horizontal 3.05 m radius semicircular array of microphones centered on the nozzle exhaust plane. The 1.27-cm omnidirectional condenser microphones used were in a plane level with the nozzle centerline. The microphones were at 60°, 90°, and 120° measured from the inlet. A mat of 15 cm thick acoustic foam was placed on the ground (asphalt) inside the microphone array to minimize ground reflections. The microphones were 1.52 m above ground level.

Microphone signals were analyzed by a 1/3-octave-band spectrum analyzer. The analyzer determined sound pressure level (SPL) spectra referenced to 2×10^{-5} N/m^2.

Acoustic measurements were taken for approximately the same jet exhaust velocities as those for the aerodynamic measurements; i.e., 200 and 259 m/sec (jet Mach numbers of 0.6 and 0.8, respectively). All flow data for the acoustic tests were taken at cold-flow, ambient temperatures near 288 K.

Model Description

Nozzle and deflectors. - The test nozzle consisted of a conical nozzle with a 5.2 cm diameter exit (fig. 2).

The deflector (fig. 2) was secured by two frames or "tracks" attached to the nozzle. The deflector could be pivoted to various angles relative to the nozzle centerline. Dimensions of the deflectors used are given also in figure 2. All deflectors had a span of 7.0 cm (1.35 times the nozzle diameter). This geometry was chosen as representative of a deflector width which could be stowable within a practical engine nacelle.

Wings. - The wings (shielding surfaces), with pertinent dimensions, are shown schematically in figure 3. The surfaces consisted of metal plates secured to wooden ribs, and were shaped to approximate the upper surface contours of the airfoils with the 20° and 60° flap settings used in reference 1. All wings had a span of 61 cm. The nozzle exit was positioned at the 0.1 chord point of each wing and at a height of 0.1 chord above the baseline wing. The 0.1 chord point is based on the wing chord with flaps retracted. The equivalent flaps-retracted chord sizes for these wings are 33 and 49.5 cm. The wings are referred to by the flap setting of 20° and 60°, and their sizes are referred to as baseline (33 cm) and 3/2-baseline (49.5 cm).

ANALYSIS

The general approach taken and considerations included in correlating the jet/flap interaction noise sources are summarized in the following sections.

Spectra

The variations of spectral shapes associated with jet/flap interaction noise (low frequencies; i.e. < 5000 Hz) for the OTW configurations tested are schematically illustrated in figure 4. The average spectra obtained for the various deflector geometries (size and angle) for each basic wing/flap combination are shown. The spectra in figure 4 are superimposed in order to illustrate local spectral shape differences; no consideration is given in the figure to actual frequencies and sound pressure levels. It is apparent that significant spectral shape differences exist for the configurations shown, particularly at lower frequencies (<1000 Hz).

Examination of the spectral plots in reference 1 suggested the individual jet/flap interaction noise sources shown in figure 5. The three sources shown are identified herein as: (1) noise caused by fluctuating

lift at the wing/flap surface (I); (2) noise associated with the jet flow at the flap trailing edge (II); and a tone-like or haystack noise source (III) thought to be related to periodic wake shedding similar to the phenomenon reported in reference 3. Hereinafter, noise source III will be referred to as wake noise. Also shown for reference in figure 5 is the nozzle-only spectral shape.

A fourth noise source that peaked in the 6-9000 Hz range (not shown in fig. 5) was evident for some configuration geometries (ref. 1). This source was identified as being associated with the deflector. The data correlation of this source is not included in this paper, which is limited to the lower frequency jet/flap interaction noise sources.

For these three jet/flap interaction noise sources (I to III), spectral shapes were evolved for each source by considering all the data of reference 1. The spectral shapes selected are given in figure 6 in terms of the reduction in sound pressure level with respect to that at the peak frequency for each source, $(SPL-SPL_p)$ as a function of 1/3-octave bands.

With the use of the spectral shapes shown in figure 6, OASPL values for each noise source were calculated for each test condition and configuration. The calculated OASPL values were then plotted as a function of the jet velocity ratio, U_M/U_j, determined from the velocity contours at the trailing edge. (Velocity profiles, in terms of local Mach numbers, normal to the trailing edge at the nozzle centerline are given in Appendix A.) A representative plot of the overall sound pressure level for the trailing edge noise source (II) as a function of U_M/U_j is given in figure 7. From such plots, parameters were evolved to correlate empirically the measured acoustic data for each noise source in terms of flow and geometry variables. These variables included jet velocity, wing size, flap setting, deflector size (streamwise length), and characteristic flow regime dimensions and velocities at the flap trailing edge. The important jet flow regime dimensions and characteristics are shown schematically in figure 8 and include the following: free shear layer thickness, δ_e, total shear layer thickness, δ^*, boundary layer thickness, δ_{BL}, peak flow velocity, U_M, and 0.5 U_M. The various jet flow thicknesses used to correlate data were obtained from the velocity profiles given in Appendix A.

Frequency

The frequencies (f_T) at which the maximum sound pressure level was obtained for each jet/flap interaction noise source are expressed by the following relationships. For the fluctuating lift noise source (I) the frequencies at the peak sound pressure levels could be correlated by ,

$$f_{I,P} = 0.216 \frac{U_j}{D} \sqrt{\frac{D}{L} (1 + \sin \alpha)} \qquad (1)$$

Similarly, for the trailing edge noise source (II),

$$f_{II,P} = 0.540 \frac{U_j}{D} \sqrt{\frac{D}{L} (1 + \sin \alpha)} \qquad (2)$$

For the wake noise source (III) the following equation was developed,

$$f_{III,P} = 0.0667 \frac{U_j}{D} \sqrt{\frac{C_a}{U_j} \sqrt{\frac{D}{L}}} \qquad (3)$$

Note that the usual Strouhal dependency on jet velocity does not occur for this noise source; rather a dependency on $\sqrt{U_j}$ was observed.

Many of the measured spectra contained a tone near 1000 Hz. This tone is believed to be associated with the natural frequency of the jet (ref. 4).

CORRELATION RESULTS

The correlation of the OTW acoustic data are presented for each noise source in the following sections. All correlations will be developed and shown at $\theta = 90^o$; the variation with radiation angle will be discussed separately. The trailing edge noise source (II) will be discussed first because this is the most important community jet/flap interaction noise source when the present data are scaled to a full-size aircraft. Then the fluctuating lift and wake noise sources (I and III, respectively) will be discussed. These latter sources appear to be less important to community noise, but can be significant with respect to structural vibration, fatigue, and cabin interior noise considerations.

Trailing-Edge Noise Source

Attached flow. - The $OASPL_{TE}$ correlation of the trailing edge noise source for a radiation angle, θ, of 90^o is shown in figure 9 as a function of the jet velocity ratio, U_M/U_j for jet Mach numbers of 0.6 and 0.8. The ordinate considers configuration size by the inclusion of two terms, the nozzle size and the wing/flap surface length. The flap setting is also included as is the jet velocity (the latter with an exponent of 7.0). Most of the data correlate on a curve given by $(U_M/U_j)^2$. The data that fall on the curve shown in figure 9 are for cases in which the jet flow over the flap is well attached to the surface at the trailing edge. The data below and to the right of the curve shown, exhibit varying degrees of jet flow separation from the flap surface. An example of this effect of partial flow separation on the acoustic characteristics is illustrated in figure 10 in which data taken from figure 9 is

identified in terms of deflector angle and the 0.5 U_M velocity contours at the flap trailing edge. With the jet flow well attached to the surface (β, 40°; circle symbol), the velocity contour is small in height above the trailing edge and spread out in the spanwise direction. As the deflector angle, β, is progressively decreased to 25°, the velocity contours increase in height and become much narrower in the spanwise direction. In particular, the deflector with a β of 25° (diamond symbol) shows significant flow separation. Thus, the relationships shown in figure 9 apply only for well attached flow, such as can be expected with flap settings in the takeoff mode (low flap angles) or with very large wing/flap chords in the landing mode (high flap angles).

Attached flow and partially separated flow. - The correlation of the trailing-edge noise source OASPL was made by consideration of the flow regimes at the trailing edge as a means to collapse the attached flow and partially separated flow data. The data reduction was directed toward obtaining a factor that included measured flow variables in the nozzle centerline plane, such as δ^*, δ_e, and δ_{BL}. These considerations came about from an examination of these variables that showed an interrelationship between them and the trailing edge velocity contour shape, δ^*/w^* (not shown).

The best correlation of the trailing edge noise source for the present configurations, is shown in figure 11. The factor correlating the acoustic data obtained with attached flow and that obtained with partially separated flow is given by:

$$F_1 = 1 + \left(7.1 \frac{\delta_{BL}}{\delta^*} \sqrt{\frac{D}{L}}\right)^4 \qquad (4)$$

where $\delta^* = \delta_e + \delta_{BL}$. With a few exceptions, very good correlation of the data ($\pm$1 dB) was obtained.

Fluctuating Lift Noise Source

Attached flow. - The $OASPL_{FL}$ correlation of the fluctuating lift noise source for $\theta = 90°$ is shown in figure 12 as a function of U_M/U_j for jet Mach numbers of 0.6 and 0.8. The ordinate is similar to that used for trailing edge noise (fig. 9); however, the exponents for U_j, L/D and α are somewhat different. Again, the data that fall on the curve shown in the figure are those with well attached flow to the flap surface at the trailing edge. Note that the U_M/U_j exponent is now 3 compared with a value of 2 for the data in figure 9. The data below and to the right of the curve show flow separation effects on acoustic characteristics similar to those discussed for figures 9 and 10.

Attached flow and partially separated flow. - The best correlation of the data with partially separated flows with that for fully attached

flows was obtained through use of the same correlation parameter, F_1, that was used to correlate the trailing edge noise source. The correlated fluctuating lift noise data are shown in figure 13 where the abscissa is again $(U_M/U_j)/(F_1)$. The data generally are correlated with ± 1.5 dB.

Wake Noise Source

Attached flow. - The $OASPL_W$ correlation of the wake noise as a function of U_M/U_j is shown in figure 14. For the most part, only the data for the 3/2-baseline wing using the 7.9-cm deflector are correlated on the 4-power slope curve shown. The remaining data, except for a few exceptions, require an additional correlation parameter to achieve collapse of the data on a single curve. It should also be noted that the data at $M_j = 0.8$ for the baseline wing with a 20° flap setting (not shown) showed little difference from that obtained with $M_j = 0.6$. The deviations of the data from the curve shown in figure 14 are again attributed to the effect of partial flow separation.

Attached flow and partially separated flow. - By considering the overall variations in acoustic characteristics, a correlation parameter was evolved that correlated the wake noise data reasonably well, except for the anomaly noted previously (baseline wing, 20° flap setting, $M_j = 0.8$). The correlation parameter selected is given by:

$$F_2 = 1 + \left(20.25 \frac{\delta_{BL}}{\delta^*} \frac{D}{L}\right)^4 \tag{5}$$

where, again, $\delta^* = \delta_e + \delta_{BL}$.

The correlation of $OASPL_W$ as a function of $(U_M/U_j)/(F_2)$ is shown in figure 15. The data, except for one point, correlate within ± 1.5 dB.

Radiation Angle

The data and correlations thus far considered are only for a radiation angle of 90°. The spectral data of reference 1 indicate that the OASPL values for the three jet/flap interaction noise sources differ at radiation angles other than 90°. The variation of the OASPL values with radiation angle, averaged for all the configurations, are shown in figure 16 as differences from the OASPL value at $\theta = 90°$ for the three noise sources. In general, the OASPL at $\theta = 60°$ was less than that at 90°, by 1½ to 3½ dB depending on the specific noise source. At $\theta = 120°$, the OASPL values were slightly higher (<1 dB) to an estimated 3 dB lower (trailing edge noise source, II) than those measured at $\theta = 90°$. The lower OASPL values were associated with a flap setting of 60° while the higher OASPL values were associated with a flap setting of 20°. It should

be noted that the trailing edge noise source OASPL valued for a flap setting of 60° is estimated because the spectra were contaminated by the jet tone at 1000 Hz and deflector noise. The latter effect on the spectra was particularly difficult to separate out at $\theta = 60^{\circ}$.

The data trends shown in figure 16 can be estimated by use of the following relationships in which the OASPL at any θ is referenced to that at $\theta = 90^{\circ}$. The variation of ΔdB with radiation angle for both the wake (III) and fluctuating lift (I) noise sources is given by:

$$\text{OASPL} - \text{OASPL}_{90^{\circ}} = 10 \log \sin^{2/a}\left[\frac{\theta}{a}\right] - 10 \log \sin^{2/a}\left[\frac{90}{a}\right] \qquad (6)$$

where

$$a = (1 + \cos^{6}\alpha)$$

The variation of OASPL - $\text{OASPL}_{90^{\circ}}$ (ΔdB) with radiation angle for the trailing edge (II) noise source is given by the same relationship as that in equation (6) except that the equation is written as 20 log rather than as 10 log.

Concluding Remarks on Source Correlation Results

The data scatter with respect to the individual noise source correlations is evident in figures 9 and 11 to 15. It is also of interest, however, to examine on a spectral basis, the data scatter of the measured configuration data with respect to the summed correlations. Typical results of such comparisons are shown in figures 17 to 20. The cases selected are for minimum and near maximum values of U_M/U_j. Minimum U_M/U_j values were generally obtained with the 7.9-cm deflector set at $\beta = 40^{\circ}$ while maximum U_M/U_j values were generally obtained with the 4.14-cm deflector set at $\beta = 25^{\circ}$ or 30°. In figures 17 to 20, the individual noise sources are shown by dashed curves and the antilogarithmic summations of the sources are shown by the solid curves. It is apparent that the summed curves compare reasonably well with the measured data, particularly for the attached flow cases. The high data point near 1000 Hz, as pointed out previously, is believed to be caused by the jet "screeching" at its natural frequency. With the 3/2-baseline wing and for some conditions with the baseline wing, the high frequency measured data are above the calculated curve because of the presence of deflector noise, the correlation of which is beyond the scope of the present work.

AEROACOUSTIC RELATIONSHIPS

From the aerodynamic data given in reference 1, the relationship of the overall OASPL for each configuration can be related to the associated

lift and thrust. Typical plots of such relationships of the overall OASPL as a function of lift, thrust, and flow turning efficiency, η are shown in figures 21 and 22 for $\theta = 90^{o}$. It is apparent that the maximum OASPL occurs, unfortunately, when the lift is maximized and the thrust is at a high level. It should be noted that the maximum thrust and flow turning efficiency, η is obtained with the separated jet/flap flow.

Specific combinations of deflector size and angle can yield the same aerodynamic performance and noise level. For example, in figure 21 consider the open-diamond symbol (30^{o}, 4.14 cm deflector) and tailed square symbol (25^{o}, 7.9 cm deflector) data. The associated trailing edge velocity profiles and noise spectra are shown in figures 23 and 24, respectively. It is apparent that the respective deflector configurations yield the same velocity profile and spectra in shape and level, thus accounting for the same aeroacoustic characteristics (lift, thrust, efficiency, and OASPL). From a practical point of view, however, the larger deflector would be heavier and more difficult to store for cruise. Thus, aeroacoustic data presented as in figures 21 and 22 can be used to assess acoustic/ aerodynamic performance trade-offs.

CONCLUDING REMARKS

On the basis of the present work it appears that the acoustic characteristics of OTW configurations using external deflectors to promote flow attachment for STOL operation can be correlated with the flow characteristics measured at the flap trailing edge and the nozzle-wing geometry. The pertinent trailing edge flow parameters are the thickness of the shear and boundary layers and the peak trailing edge velocity. The geometry parameters include the shielding surface length, deflector size, and flap setting.

Specific combinations of deflector geometry (size and angle) can reduce the jet/flap interaction noise level; however, the aerodynamic performance, based on static lift and thrust measurements, are adversely affected. In general, the best aerodynamic performance for STOL is accompanied by the highest jet/flap interaction noise level.

APPENDIX A - TRAILING EDGE VELOCITY PROFILES

From jet flow Mach number contour plots made normal to the flap trailing edge (unpublished data) velocity profiles were developed at the nozzle centerline. The procedural details used in obtaining these contour plots are given in reference 5. The resulting velocity profiles, in terms of local Mach number, are shown in figures A-1 and A-2. These velocity profiles for the various wing/flap/deflector configurations were used to obtain values of δ_{BL}, δ^{*}, δ_{e}, U_{M}, and 0.5 U_{M}. These values, as appropriate, were then used in the data correlations.

The onset of partially separated flow is evident in the data from a significant thickening of the boundary and shear layers at a given deflector angle (or flap setting) compared to other profiles in the same configuration category.

Trends readily apparent from the data in figures A-1 and A-2 indicate that: (1) the peak velocity at the flap trailing edge decreases with an increase in wing size and deflector angle; (2) the larger deflector tends to delay flow separation; (3) the trailing edge peak velocity generally decreases with an increase in flap setting; and finally, (4) the overall shear layer thickness increases with an increase in flap setting.

NOMENCLATURE

A	nozzle exhaust area, cm^2
C	wing chord (flaps retracted)
D	nozzle exhaust diameter
F_1, F_2	flow separation parameters (defined in text)
f_p	peak 1/3-octave band frequency for a given noise source
L	shielding surface length
L_f	wing length upstream of nozzle exhaust plane
L_p	projected shielding surface length
L_T	lift
ℓ	effective deflector length
M	local jet flow Mach number
M_j	jet exhaust Mach number
OASPL	overall sound pressure level, dB re 2×10^{-5} N/m^2
$OASPL_C$	configuration overall sound pressure level, dB re 2×10^{-5} N/m^2
$OASPL_{FL}$	fluctuating lift noise source (I) OASPL, dB re 2×10^{-5} N/m^2
$OASPL_{TE}$	trailing edge noise source (II) OASPL, dB re 2×10^{-5} N/m^2
$OASPL_W$	wake noise source (III) OASPL, dB re 2×10^{-5} N/m^2

SPL	sound pressure level, dB re 2×10^{-5} N/m^2
SPL_P	peak sound pressure level, dB re 2×10^{-5} N/m^2
T	thrust
T_j	jet thrust, nozzle alone
U_j	jet exhaust velocity
U_M	maximum jet velocity at flap trailing edge
w*	spanwise width of 0.5 U_M contour measured at trailing edge
α	flap setting (angle)
β	deflector angle
δ	characteristic jet effux thickness at trailing edge (nozzle centerline). See figure 8.
δ_{BL}	boundary layer thickness at trailing edge. See figure 8.
δ_e	free shear layer thickness at trailing edge. See figure 8.
δ^*	characteristic shear layer thickness at 0.5 U_M at trailing edge. See figure 8.
η	flow turning efficiency, $\sqrt{\frac{(L_T)^2 - T^2}{T_j^2}}$
θ	acoustic radiation angle measured from nozzle inlet
I,II,III	jet/flap interaction noise source identifications

REFERENCES

1. von Glahn, U. and Groesbeck, D., "Effect of External Jet-Flow Deflector Geometry on OTW Aero-Acoustic Characteristics," NASA TM X-73460, 1976.

2. Reshotko, M. and Friedman, R., "Acoustic Investigation of the Engine-Over-the-Wing Concept Using a D-Shaped Nozzle," AIAA Paper 73-1030, Seattle, Wash., 1973.

3. Schlinker, R. H., Amiet, R. K., and Fink, M. R., "Vortex Noise from Nonrotating Cylinders and Airfoils," AIAA Paper 76-81, Washington, D.C., 1976.

4. Neuwerth, G., "Acoustic Feedback Phenomena of the Subsonic and Hypersonic Free Jet Impinging on a Foreign Body," NASA TT F-15719, 1974.

5. von Glahn, U. and Groesbeck, D., "Geometry Effects on STOL Engine-Over-the-Wing Acoustics with 5:1 Slot Nozzles," NASA TM X-71820, 1975.

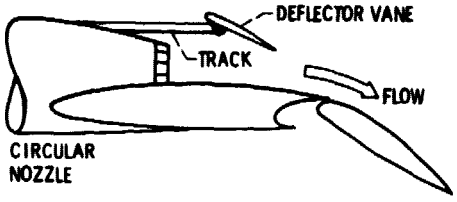

Figure 1. - Nozzle-off-wing with external deflector.

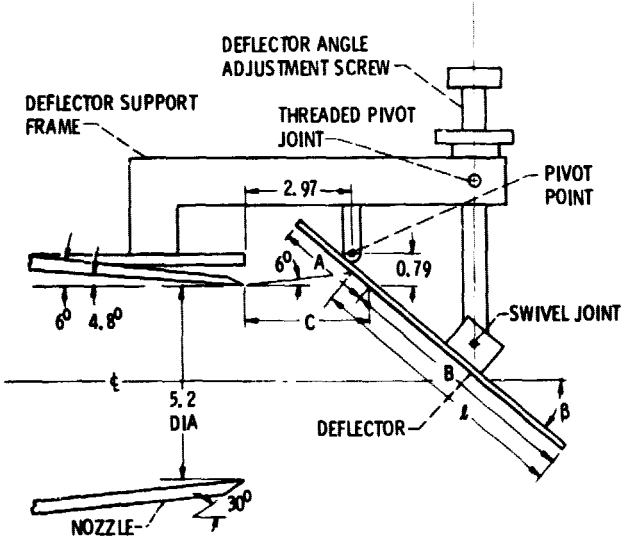

ℓ	A	B	C	β
4.14	2.51	3.18	3.91	20°
	2.29	3.40	3.66	25°
	2.18	3.51	3.51	30°
	2.06	3.63	3.25	40°
7.90	2.54	6.91	4.01	20°
	2.31	7.14	3.66	25°
	2.11	7.34	3.40	30°
	2.03	7.42	3.18	40°

Figure 2. - Schematic sketch of nozzle and flow deflector. (All dimensions in centimeters.)

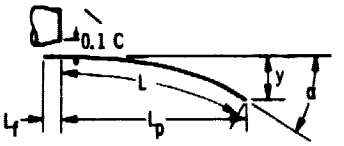

WING DIMENSIONS

FLAP ANGLE, α, DEG	CONFIGURATION	y, CM	L_f, CM	L_p, CM	L, CM
20	BASELINE	6.6	3.3	[illegible]	39.0
	3/2-BASELINE	10.2	5.0	56.0	58.4
60	BASELINE	14.3	3.3	34.1	42.3
	3/2-BASELINE	21.5	5.0	50.9	62.8

Figure 3. - Wing dimensions.

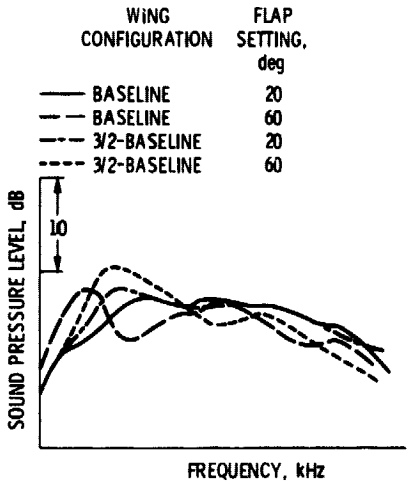

Figure 4. - Averaged spectra for frequencies less than 5000 Hz superimposed to illustrate configuration effects on spectral shape.

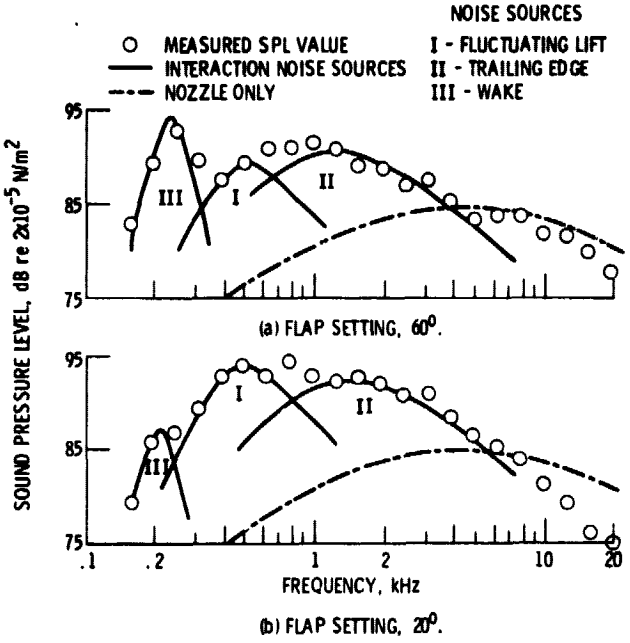

Figure 5. - Jet/surface interaction noise source identifications. Baseline wing; M_j, 0.8; deflector length, 7.9 cm; deflector angle, 25°; θ, 90°.

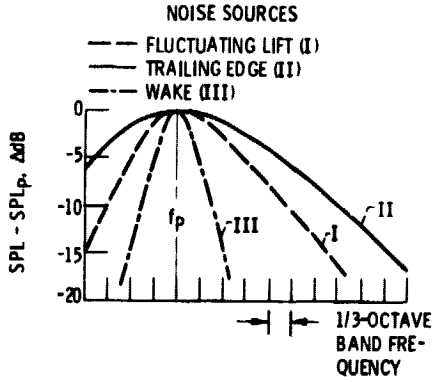

Figure 6. - Jet/surface interaction noise source spectral characteristics.

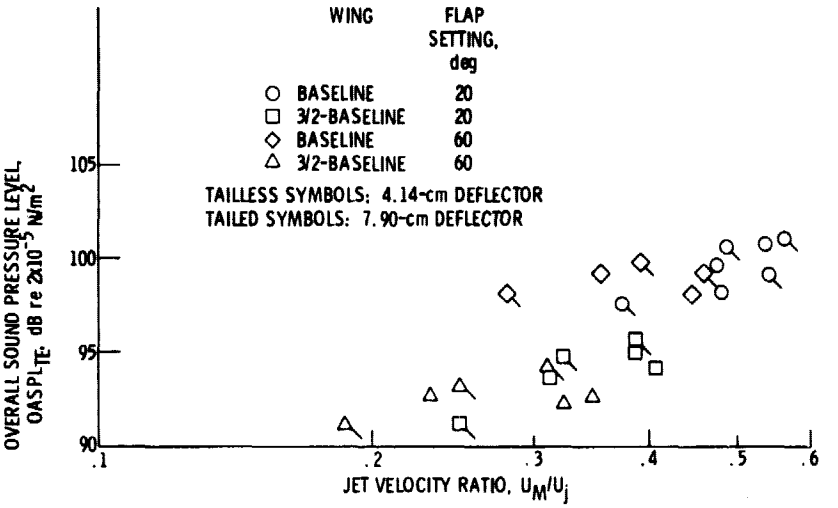

Figure 7. - Variation of trailing-edge OASPL with trailing-edge velocity ratio for various configuration geometries. M_j, 0.8; θ, 90°.

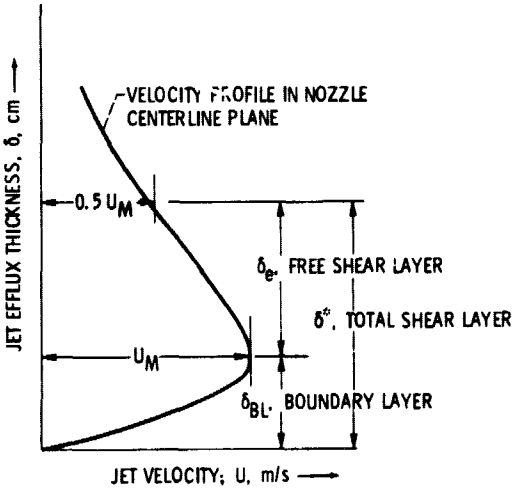

Figure 8. - Flow regime dimensions at flap trailing edge.

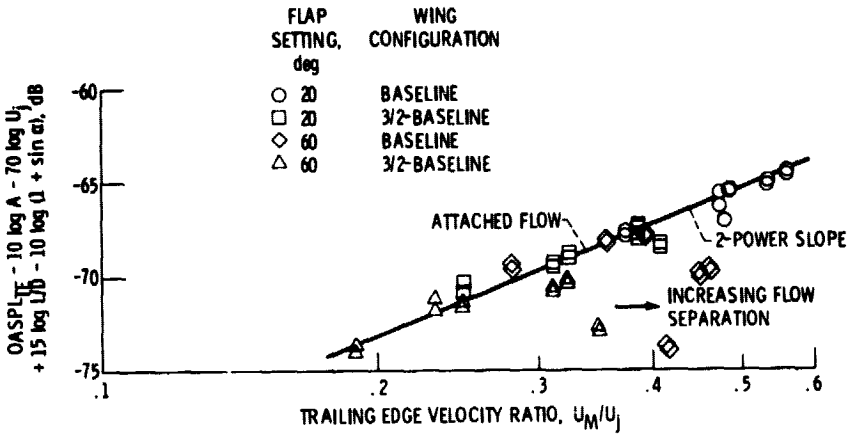

Figure 9. - Correlation of trailing-edge noise source OASPL as a function of trailing edge velocity ratio. M_j, 0.6 and 0.8; θ, 90°.

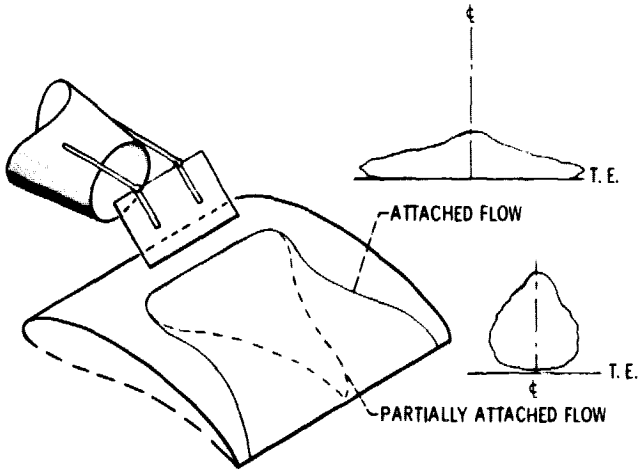

(a) SCHEMATIC SKETCH OF REPRESENTATIVE JET FLOW PATTERNS OVER WING/ FLAP SURFACE.

Figure 10. - Representative changes in trailing edge contours (0.5 U_M) associated with acoustic changes for varying degrees of separated flow. Baseline wing; flap setting, 60°; trailing edge noise source; M_j, 0.8; L/D, 0.8; θ, 90°.

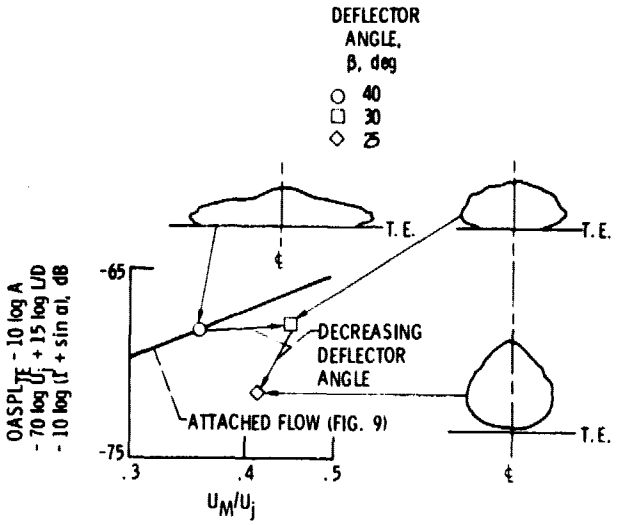

(b) RELATIONSHIP OF FLOW PATTERNS TO ACOUSTICS.

Figure 10. - Concluded.

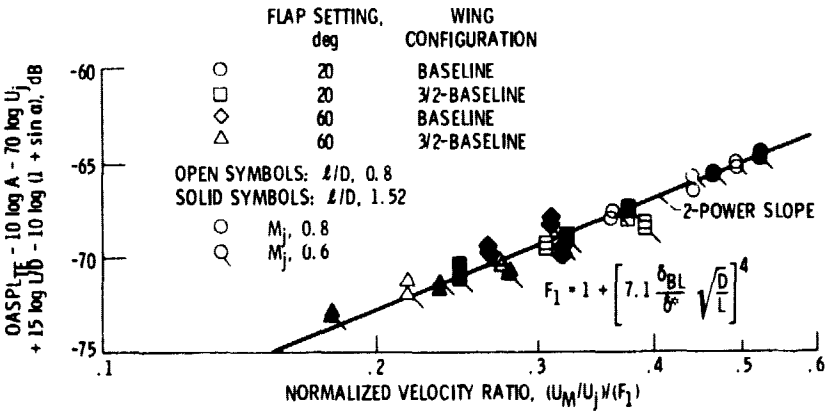

Figure 11. - Correlation of trailing edge noise source OASPL for attached and partially separated flows. θ, 90°.

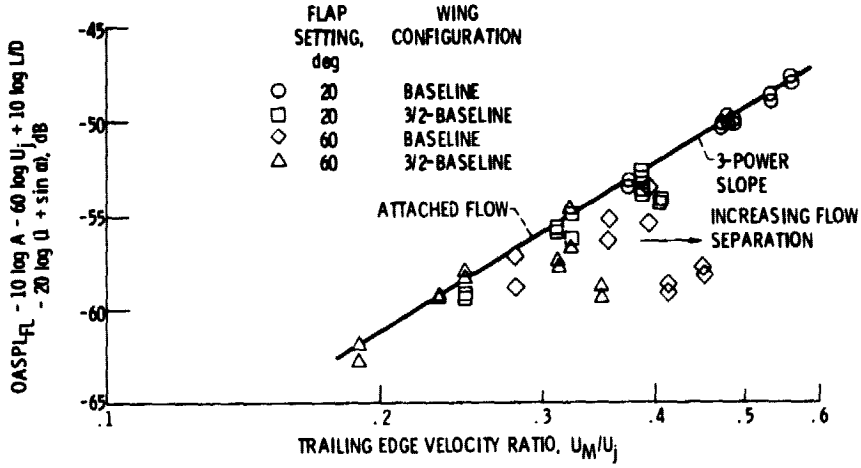

Figure 12. - Correlation of fluctuating lift noise source OASPL as a function of trailing edge velocity ratio. M_j, 0.6 and 0.8; θ, 90^0.

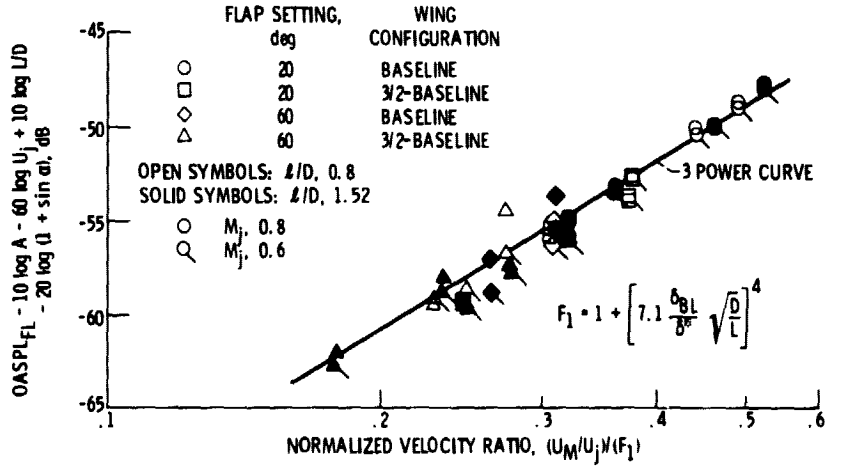

Figure 13. - Correlation of fluctuating lift noise source OASPL for attached and partially separated flows. θ, 90^0.

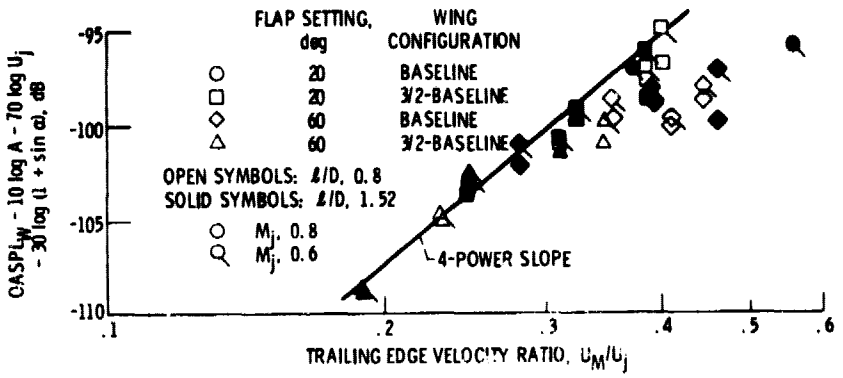

Figure 14. - Correlation of wake noise source OASPL as a function of trailing-edge velocity ratio. θ, 90°.

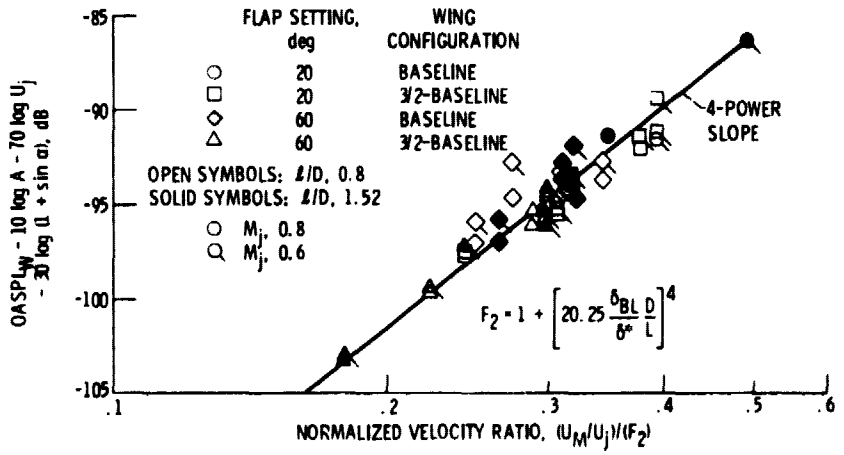

Figure 15. - Correlation of wake noise source OASPL for attached and partially separated separated flows. θ, 90°.

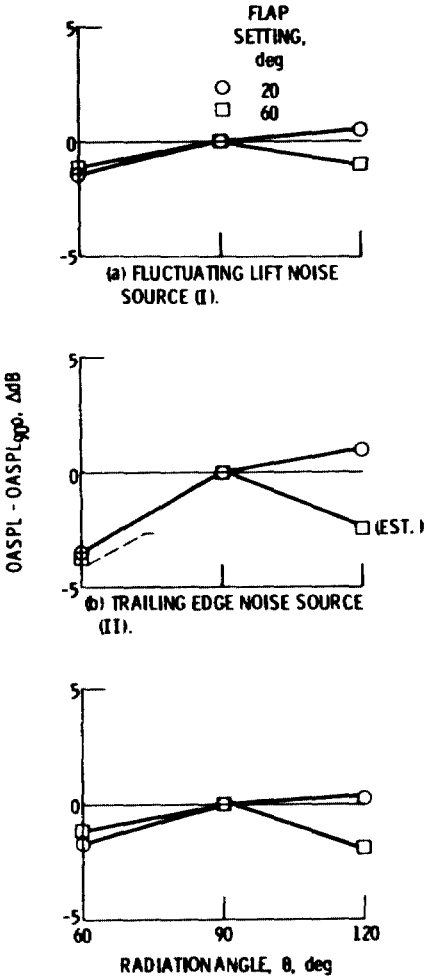

Figure 16. - OASPL variation with radiation angle.

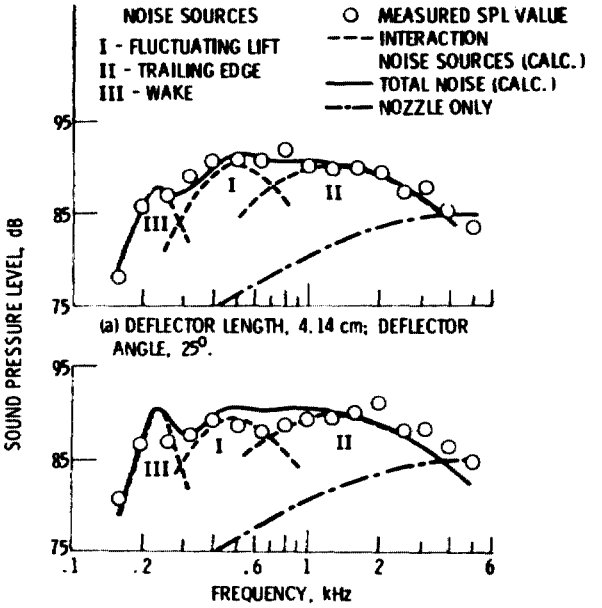

Figure 17. - Comparison of representative measured and predicted interaction noise spectra. Baseline wing; flap setting, 20°; M_j, 0.8; θ, 90°.

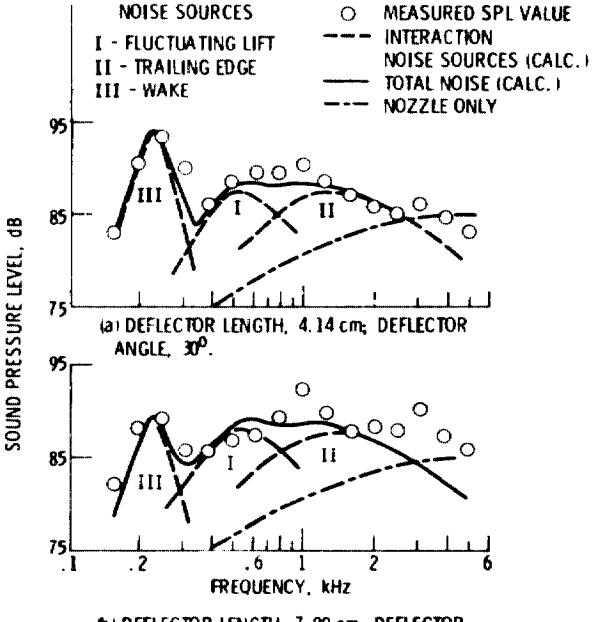

(a) DEFLECTOR LENGTH, 4.14 cm; DEFLECTOR ANGLE, 30^{0}.

(b) DEFLECTOR LENGTH, 7.90 cm; DEFLECTOR ANGLE, 40^{0}.

Figure 18. - Comparison of representative measured and predicted interaction noise spectra. Baseline wing; flap setting, 60^{0}; M_j, 0.8; θ, 90^{0}.

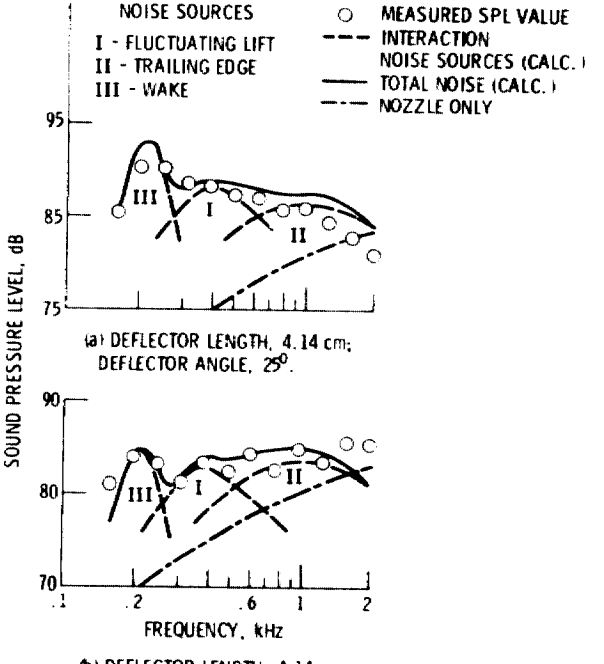

(a) DEFLECTOR LENGTH, 4.14 cm; DEFLECTOR ANGLE, 25^{0}.

(b) DEFLECTOR LENGTH, 4.14 cm; DEFLECTOR ANGLE, 40^{0}.

Figure 19. - Comparison of representative measured and predicted interaction noise spectra. 3/2-baseline wing; flap setting, 20^{0}; M_j, 0.8; θ, 90^{0}.

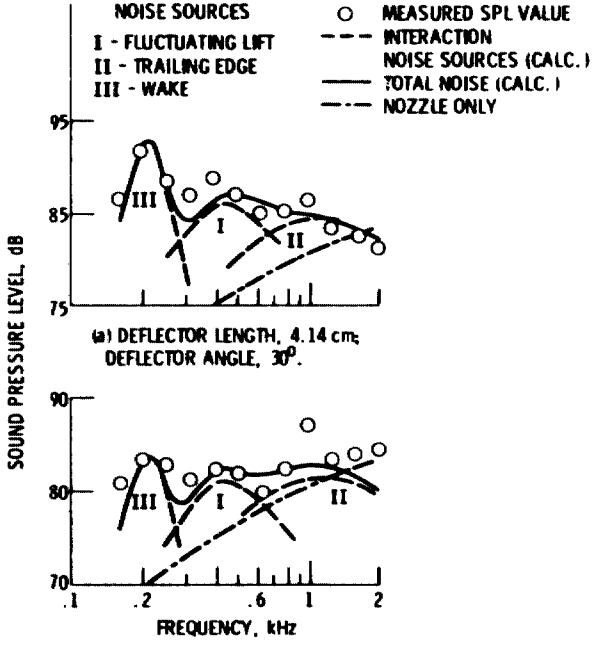

(a) DEFLECTOR LENGTH, 4.14 cm; DEFLECTOR ANGLE, 30°.

(b) DEFLECTOR LENGTH, 7.90 cm; DEFLECTOR ANGLE, 40°.

Figure 20. - Comparison of representative measured and predicted interaction noise spectra. 3/2-baseline wing; flap setting, 60°; M_j, 0.8; θ, 90°.

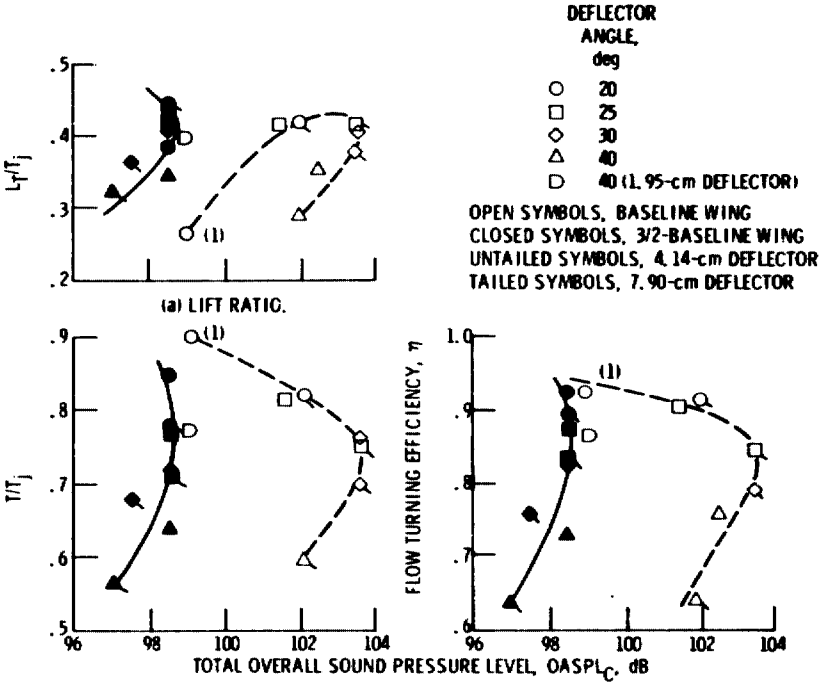

(a) LIFT RATIO.

(b) THRUST RATIO.

(c) FLOW TURNING EFFICIENCY.

Figure 21. - Aeroacoustic performance summary with 20° flap setting. M_j, 0.8; θ, 90°.

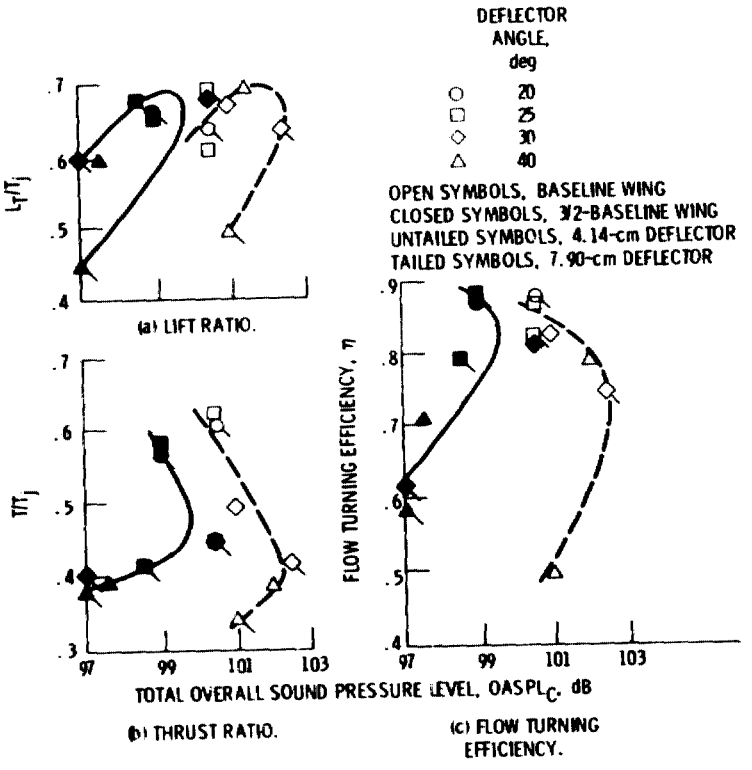

Figure 22. - Aeroacoustic performance summary with 60^0 flap setting. M_j, 0.8; θ, 90^0.

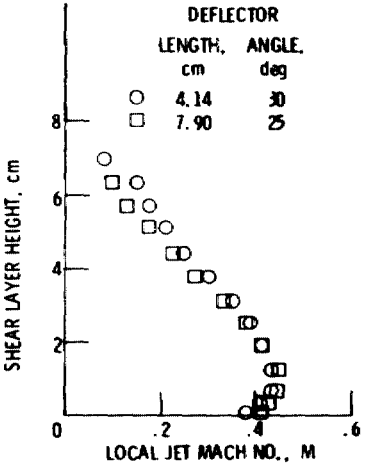

Figure 23. - Centerline velocity profile at flap trailing edge. M_j, 0.8, flap setting, 20^0; baseline wing.

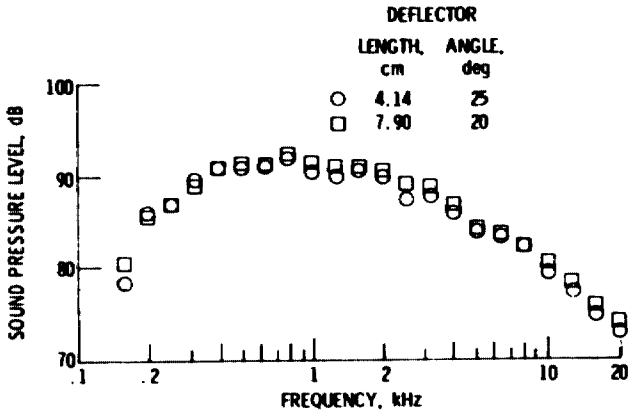

Figure 24. - Comparison of spectra obtained with two different deflectors at nearly equal configuration lift and thrust values. Flap setting, 25°; baseline wing; M_j, 0.8; θ, 90°.

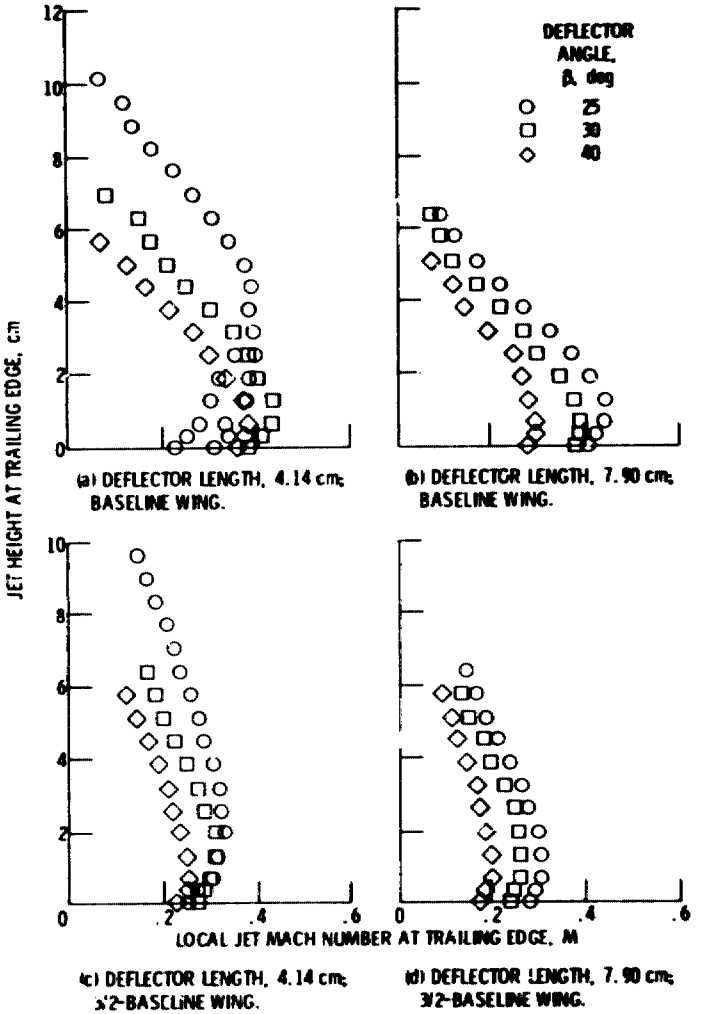

Figure A-1. - Trailing edge velocity profiles at nozzle centerline. Flap setting, 20°; M_j, 0.8.

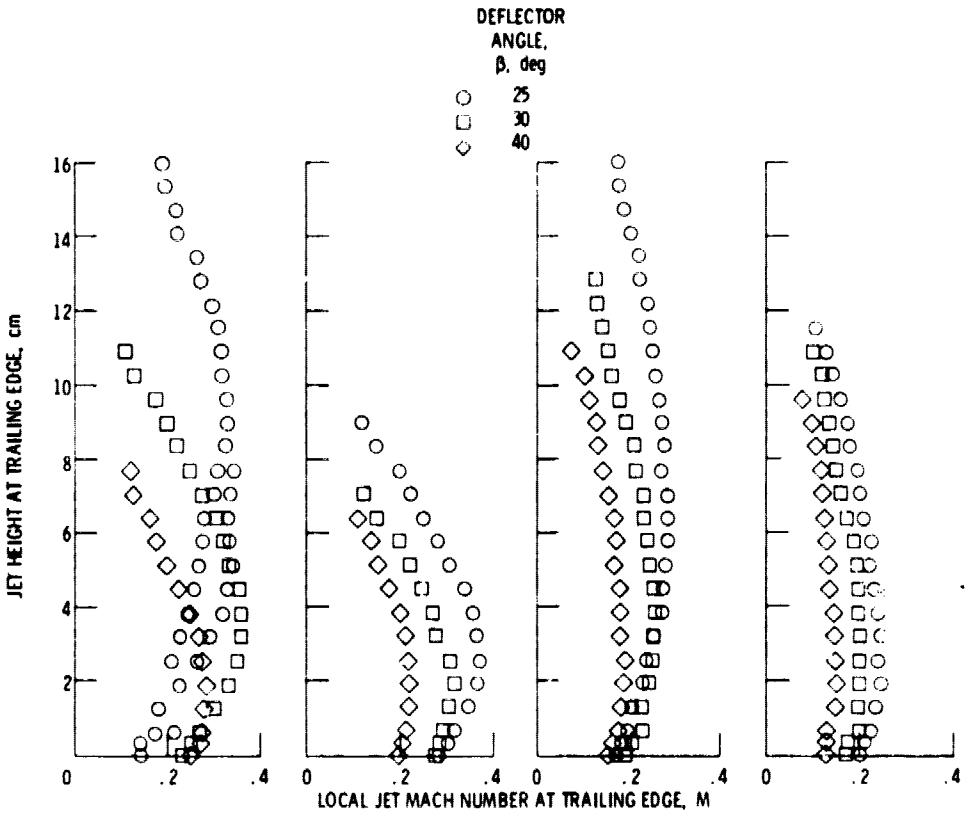

Figure A-2. - Trailing edge velocity profiles at nozzle centerline. Flap setting, 60^0; M_j, 0.8.